JACS
JOURNAL OF THE AMERICAN CHEMICAL SOCIETY
Article
Cite This: J. Am. Chem. Soc. XXXX, XXX, XXX−XXX
pubs.acs.org/JACS

Supramolecular Control of Azobenzene Switching on Nanoparticles

Zonglin Chu,[†] Yanxiao Han,[‡] Tong Bian,[†] Soumen De,[†] Petr Král,[‡,§] and Rafal Klajn*[,†]

[†]Department of Organic Chemistry, Weizmann Institute of Science, Rehovot 76100, Israel
[‡]Department of Chemistry, University of Illinois at Chicago, Chicago, Illinois 60607, United States
[§]Department of Physics and Department of Biopharmaceutical Sciences, University of Illinois at Chicago, Chicago, Illinois 60607, United States

Supporting Information

ABSTRACT: The reversible photoisomerization of azobenzene has been utilized to construct a plethora of systems in which optical, electronic, catalytic, and other properties can be controlled by light. However, owing to azobenzene's hydrophobic nature, most of these examples have been realized only in organic solvents, and systems operating in water are relatively scarce. Here, we show that by coadsorbing the inherently hydrophobic azobenzenes with water-solubilizing ligands on the same nanoparticulate platforms, it is possible to render them essentially water-soluble. To this end, we developed a modified nanoparticle functionalization procedure allowing us to precisely fine-tune the amount of azobenzene on the functionalized nanoparticles. Molecular dynamics simulations helped us to identify two distinct supramolecular architectures (depending on the length of the background ligand) on these nanoparticles, which can explain their excellent aqueous solubilities. Azobenzenes adsorbed on these water-soluble nanoparticles exhibit highly reversible photoisomerization upon exposure to UV and visible light. Importantly, the mixed-monolayer approach allowed us to systematically investigate how the background ligand affects the switching properties of azobenzene. We found that the nature of the background ligand has a profound effect on the kinetics of azobenzene switching. For example, a hydroxy-terminated background ligand is capable of accelerating the back-isomerization reaction by more than 6000-fold. These results pave the way toward the development of novel light-responsive nanomaterials operating in aqueous media and, in the long run, in biological environments.

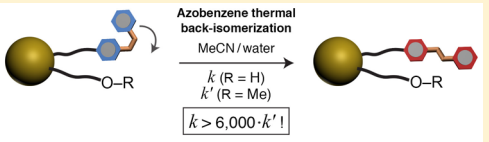

INTRODUCTION

The reversible isomerization of azobenzene (1,2-diphenyldiazene)—one of the simplest and most robust photoswitchable compounds—has been investigated extensively for nearly a century.[1] The *trans*−*cis* isomerization process entails a significant change in the shape of the molecule and a decrease in the distance between two *para* substituents from ∼9 Å to ∼6.5 Å. These changes in various azobenzene derivatives have been used to modulate catalysis,[2−4] affinity to metal ions,[5] and binding to biological molecules in living organisms[6,7] and even to control the conformation of a bound "guest" molecule.[8] However, whereas all of these functions have been realized in free molecules, the immediate surroundings of a molecular switch can have a profound effect on its switching properties. It has long been known, for example, that confining azobenzenes within small volumes can effectively suppress their switching[9−14] and that the success of *trans* → *cis* isomerization could be correlated[15] to the amount of free space available to an azobenzene unit. In contrast, several systems showed evidence of cooperative azobenzene switching,[16−18] whereby densely packed azobenzenes isomerized very readily in a process most likely initiated at the periphery of an ensemble.[19,20] Beyond these single-component systems, it would arguably be more interesting to control the properties of molecular switches by other species residing in their proximity.

Inorganic nanoparticles (NPs) functionalized with binary (mixed) monolayers of ligands[21−25] provide an attractive platform for inducing intermolecular interactions between the adsorbed species and hence for investigating how various functional groups affect the properties of switchable molecules. An additional advantage of the mixed-monolayer approach is that by decorating NPs with mixtures of functional and solubilizing ligands, it becomes possible, by tuning the composition of the monolayer,[26] to effectively solubilize compounds that are otherwise insoluble in a given solvent.[27] For example, whereas azobenzene-functionalized NPs have been investigated extensively in various organic solvents,[28−32] their properties in aqueous media have remained unknown because of the nonpolar nature of azobenzene and, consequently, the very low solubility of azobenzene-functionalized NPs in water. Access to water-soluble, azobenzene-coated NPs could broaden the scope of applications of these nanomaterials, in particular in the context of biomedical applications (such as in photopharmacology[33,34]).

We hypothesized that water-soluble, azobenzene-coated NPs could be obtained by functionalizing NPs with mixed monolayers comprising (i) azobenzene and (ii) a ligand terminated with a polar group, such as an oligo(ethylene)

Received: September 6, 2018
Published: December 31, 2018

DOI: 10.1021/jacs.8b09638
J. Am. Chem. Soc. XXXX, XXX, XXX−XXX

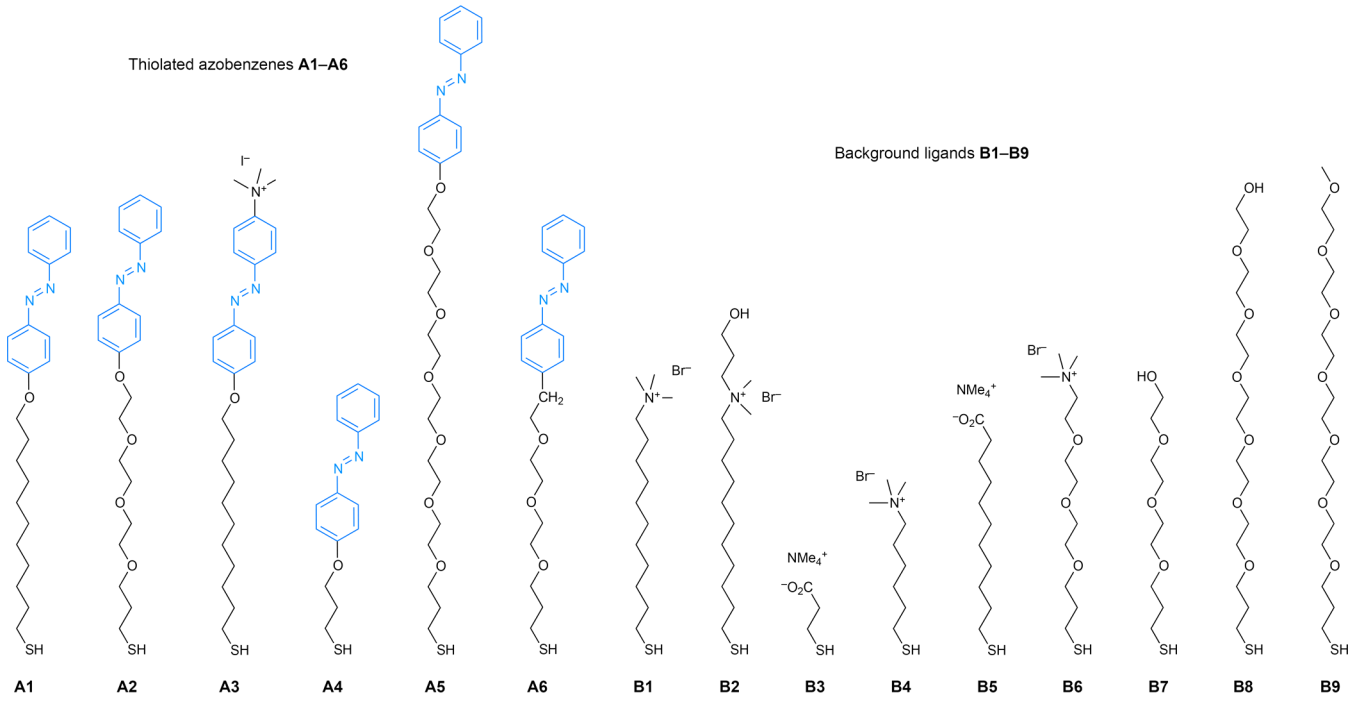

Figure 1. Structural formulas of thiolate ligands used in this study.

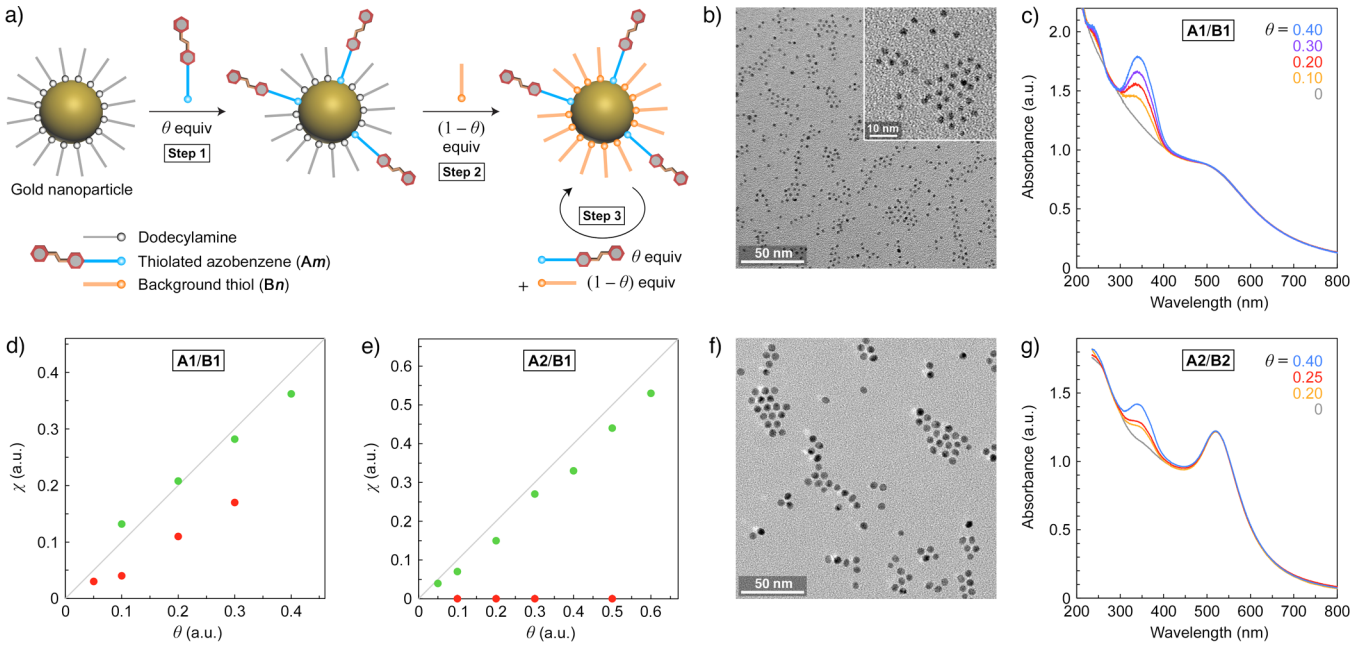

Figure 2. (a) Schematic illustration of the three-step procedure adopted in this study. (b) Representative transmission electron microscopy (TEM) image of **A1**/**B1**-functionalized 2.5 nm Au NPs (θ = 0.30) deposited on a carbon-coated copper grid from an aqueous solution. (c) Series of UV/vis absorption spectra of **A1**/**B1**-functionalized 2.5 nm Au NPs (in water) obtained at different θ values. (d) Dependence of the on-NP molar fraction of azobenzene **A1**, χ, on its molar fraction used in the functionalization step, θ. The red and the green markers correspond to functionalization by the simultaneous and consecutive addition of the two thiols, respectively. The gray line corresponds to $\theta = \chi$. (e) Dependence of χ on θ for the **A2** + **B1** combination. (f) Representative TEM image of **A2**/**B2**-functionalized 5.5 nm Au NPs (χ = 0.15). (g) Series of UV/vis absorption spectra of **A2**/**B2**-functionalized 5.5 nm Au NPs (in 9:1 v/v water−methanol) obtained at different θ values. Note the pronounced band at ∼520 nm due to the localized surface plasmon resonance of 5.5 nm Au NPs.

glycol (OEG) chain or a charged group. Such functionalization is typically achieved by treating NPs capped with weakly bound ligands (e.g., dodecylamine (DDA) for Au NPs) with an excess of ligands having higher affinity (e.g., thiols). We speculated that above a critical fractional coverage with polar ligands the NPs should be soluble in water despite the presence of the hydrophobic azobenzene groups. However, cofunctionalization of NPs with mixtures of polar and apolar ligands is not an easy task:[24] earlier studies showed that such processes typically result in preferential adsorption of only one of the two ligands. Among numerous other examples,[35−40] Bishop and co-workers found that performing ligand exchange

DOI: 10.1021/jacs.8b09638
J. Am. Chem. Soc. XXXX, XXX, XXX−XXX

on DDA-capped 6 nm Au NPs with an 8:1 mixture of octadecanethiol and ω-mercaptoundecanoic acid resulted in a 0.35:1 mixture of these two ligands on the functionalized NPs,[41] whereas Meli et al. reported that a 3:1 molar ratio of dodecanethiol and ω-mercaptoundecanol used to functionalize 4 nm NPs was increased up to 32:1 as a result of the ligand exchange reaction.[42] The discrepancy between the solution and the on-NP ratio typically originates from attractive/repulsive interactions between the ligands or when one of the ligands induces NP precipitation during the functionalization process. Therefore, we developed a modified NP functionalization procedure that allowed us to predictably control the molar ratio of the two ligands on the NPs. These NPs allowed us to systematically investigate how the background ligand influenced the switching properties of azobenzene in water.

RESULTS AND DISCUSSION

Controlling the Fractional Coverage of Azobenzene on Water-Soluble Nanoparticles. We functionalized gold NPs with different combinations of thiolated azobenzenes **A*m*** (***m*** = 1 through 6) and background ("dummy") thiols **B*n*** (***n*** = 1 through 9) (Figure 1 and Supporting Information, Sections 2−4) using the following approach. First, we treated DDA-capped NPs with θ (where $\theta < 1$) equivalents of **A*m*** (step 1 in Figure 2a; equiv with respect to the number of binding sites on the NPs, calculated assuming that a single thiolate moiety occupies an area of 0.214 nm^2 on the surface of gold[43]). After 1 h, $(1 - \theta)$ equiv of **B*n*** was added and shaking was continued for an additional 2 h (Figure 2a, step 2). This two-step procedure should lead to a practically quantitative ligand exchange, given alkanethiols' ∼100 times higher (vs alkyl amines) affinity to gold.[13] To ensure that the ligand exchange reaction was complete, we then added one extra equivalent of thiol (i.e., a mixture of θ equiv of **A*m*** and $(1 - \theta)$ equiv of **B*n***) (step 3 in Figure 2a). After ∼1 h of mixing, the functionalized NPs were washed, dried, and dissolved in deionized water (see Supporting Information, Section 4.1.2, for details).

Figure 2b shows a representative transmission electron microscopy (TEM) image of **A1**/**B1**-functionalized 2.5 nm NPs. Comparing TEM images before and after ligand exchange allowed us to conclude that our functionalization protocol did not affect the size or size distribution of the NPs. (A valid question is whether the three-step functionalization procedure yields monolayers of intermixed ligands, as opposed to patches of azobenzene and background thiol;[44] we will address this issue later, with several observations supporting the former scenario.) UV/vis absorption spectra of aqueous solutions of **A1**/**B1**-functionalized NPs obtained with increasing values of θ displayed increasing absorption at ∼350 nm (due to the $\pi \rightarrow \pi^*$ transition of *trans*-azobenzene, Figure 2c). We found that NPs prepared with as much as $\theta = 0.4$ exhibited excellent aqueous solubility (with no signs of NP aggregation by TEM, dynamic light scattering (DLS), or UV/vis absorption spectroscopy). When $\theta > 0.4$, however, the NPs could not be redispersed in water owing to the hydrophobic character of the terminal azobenzene groups.

To determine the actual molar fraction of **A1** on the functionalized NPs (i.e., χ), we subtracted the spectrum of 2.5 nm NPs functionalized with a single-component monolayer of **B1** (gray in Figure 2c) from the spectra of **A1**/**B1**-decorated NPs. Provided that the background ligand **B1** exhibits no absorption in the near-UV and visible range, the operation afforded the optical response of pure **A1**, based on which its concentration could be evaluated (see Supporting Information, Section 5). The green markers in Figure 2d denote the dependence of χ on θ for NPs functionalized by the consecutive addition of the two thiols. With an average deviation of ∼11% (based on the four data points), this method allows us to predictably control the fractional coverage of azobenzene on Au NPs. In contrast, the simultaneous addition of **A1** and **B1** led to a much higher deviation of ∼94% (Figure 2d, red markers).

Having demonstrated the ability to control the amount of **A1** on the surfaces of NPs, we sought approaches to further (i.e., beyond $\chi = 0.36$) increase the loading of azobenzene on Au NPs while keeping the particles soluble in water. First, we replaced **A1**'s alkyl chain with the hydrophilic tris(ethylene glycol) to afford **A2** (Figure 1). With the same background ligand **B1**, the molar fraction of **A2** on 2.5 nm water-soluble NPs could be increased up to $\chi \approx 0.53$ (Figure 2e). The **A2**/**B1** combination emphasized the usefulness of the three-step NP functionalization protocol adopted in this work; as the red markers in Figure 2e show, treating 2.5 nm NPs simultaneously with a mixture of 5 equiv of **A2** and 5 equiv of **B1** resulted in NPs on which no **A2** could be detected. On the other hand, following the modified protocol allowed us to place desired amounts of **A2** on the NPs, with an average deviation (from $\theta = \chi$) of only ∼23% (Figure 2e, green markers). We also synthesized **A3**, which contains an extra quaternary ammonium group at the 4′ position of azobenzene. This presence of this highly polar group allowed us to further increase the molar fraction of azobenzene on Au NPs to $\chi = 0.84$ (see Supporting Information, Figure S56b).

To verify the applicability of our functionalization protocol to NPs of other sizes, we worked with 5.5 nm, DDA-capped Au NPs. Similar to 2.5 nm NPs, these larger particles could be readily functionalized with different **A*m***/**B*n*** mixtures such that the resulting χ approached the expected θ value (see Supporting Information, Section 4.2.1, for details). For example, the **A1**:**B1** ratio on the NPs differed by only ∼12% from the expected one (average value based on three samples). To further demonstrate the proof-of-concept, we worked with a mixture of **A2** and a newly synthesized polar ligand, **B2**. Figure 2f shows a representative TEM image of **A2**/**B2**-functionalized NPs at $\theta = 0.20$ (corresponding to $\chi = 0.15$), and the UV/vis spectra in Figure 2g correspond to NPs decorated with three different **A2**:**B2** ratios. Based on these three samples, we determined the average deviation from $\theta = \chi$ to be ∼14%. Experiments with multiple other **A*m***/**B*n*** combinations confirmed that our functionalization procedure allows us to control the molar fraction of azobenzene on both 2.5 and 5.5 nm NPs.

Reversible Isomerization of Azobenzene on Water-Soluble Nanoparticles. It was of critical importance to verify that azobenzenes adsorbed on the surfaces of gold NPs retain their photoswitchable properties. Figure 3a shows changes in the UV/vis spectra of **A1**/**B1**-functionalized 2.5 nm NPs ($\chi = 0.17$) resulting from exposure to a low-intensity (∼0.7 $mW \cdot cm^{-2}$) hand-held UV light source. Within several minutes of UV irradiation, the band at ∼350 nm decreased nearly to the background level, indicative of *trans* → *cis* azobenzene isomerization. Notably, azobenzene switching did not affect the high colloidal stability of the NPs (no absorption increase in the long-wavelength region, Figure 3a). Therefore, these NPs behave differently than the azobenzene-coated NPs do in hydrophobic solvents, which, upon UV irradiation, readily

DOI: 10.1021/jacs.8b09638
J. Am. Chem. Soc. XXXX, XXX, XXX−XXX

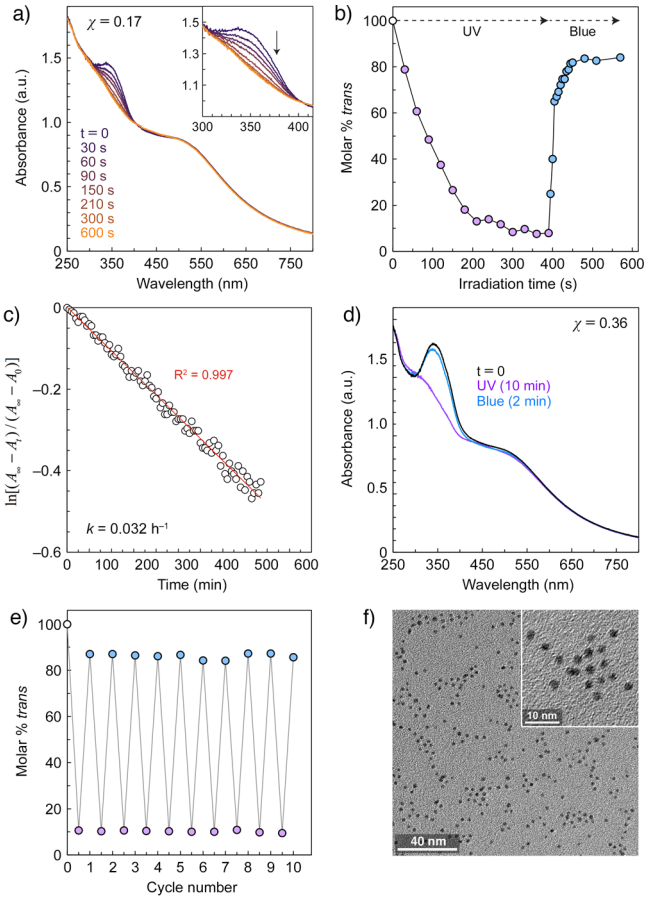

Figure 3. (a) Evolution of the UV/vis absorption spectra of an aqueous solution of **A1**/**B1**-functionalized 2.5 nm Au NPs (χ = 0.17) under UV light exposure. (b) Reversible photoswitching of **A1** on **A1**/**B1**-functionalized 2.5 nm Au NPs. (c) Kinetics of the thermal back-isomerization of **A1** on the same NPs (A_∞ denotes the absorbance at λ_{max} before irradiation; A_0, immediately after an extended exposure to UV light; A_t, after thermal relaxation for time t; k, rate constant). (d) UV/vis absorption spectra of an aqueous solution of **A1**/**B1**-functionalized 2.5 nm NPs (at χ = 0.36) before (black) and after (purple) exposure to UV light and after subsequent exposure to blue light (in blue). (e) Reversible switching of azobenzene for 10 cycles (10 min of UV and 1 min of blue light irradiation were applied in each cycle (χ = 0.36)). (f) Representative TEM image of χ = 0.36 **A1**/**B1**-functionalized 2.5 nm Au NPs after 10 switching cycles.

assemble into metastable aggregates to minimize contact with the nonpolar environment.[30,45,46]

To accurately determine the photoisomerization yield of azobenzene on NPs, we developed a procedure based on a combination of UV/vis absorption and NMR spectroscopies (see Section 6 of the Supporting Information for details). Using this method, we found that the photostationary state (PSS) under UV light contained ~92% of the *cis* isomer (Figure 3b). Subsequent exposure to blue light (we worked with a 460 nm light-emitting diode) triggered a fast back-isomerization reaction; the PSS was reached within <2 min, and it consisted of ~84% *trans*-azobenzene. We also studied the kinetics of spontaneous back-isomerization (relaxation) in the dark (Figure 3c). Kinetic analysis of the reaction, performed by monitoring the increase in absorbance at 350 nm, revealed that the reaction obeyed first-order kinetics, with a rate constant of $k \approx 0.032\ h^{-1}$, a value typical of **A1** and other structurally simple azobenzenes in organic solvents. Nanoparticles functionalized with higher amounts of **A1** behaved analogously; for example, UV irradiation of χ = 0.36 NPs allowed us to establish a PSS with ~90% *cis*-**A1** within a similar time scale of several minutes (Figure 3d; see also Figures S59–S61 in the Supporting Information). Importantly, the system was highly reversible (Figure 3e), and repeated switching of azobenzene on the NPs did not affect their size distribution (Figure 3f).

To help better understand the high solubility and efficient switching of **A1**/**B1**-functionalized NPs in water, we studied these particles by means of atomistic molecular dynamics (MD) simulations. In these studies, an icosahedral[47−49] gold nanoparticle functionalized with a densely packed monolayer of randomly distributed *trans*-**A1** and background ligands **B1** was first constructed. The size of the metallic core was ~2.5 nm, and χ amounted to 0.15 (which corresponds to 14 **A1** ligands and 77 **B1** ligands; Figure 4a, left), in agreement with a

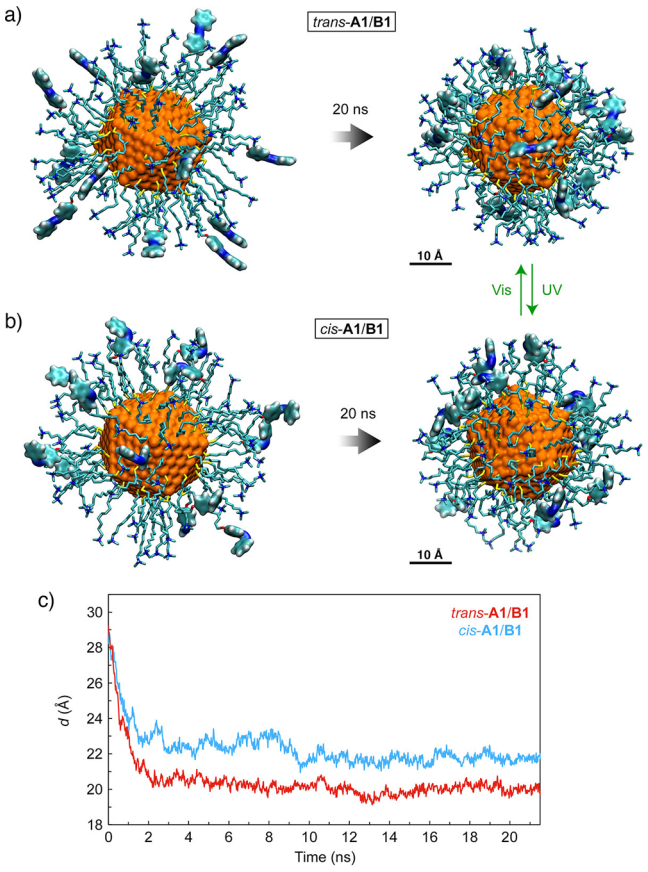

Figure 4. Snapshots from molecular dynamics (MD) simulations of an **A1**/**B1**-coated gold NP in the *trans* (a) and *cis* (b) state of azobenzene. The images on the left correspond to t = 0, and those on the right correspond to t = 20 ns. Color codes: C, cyan; N, blue; O, red; S, yellow. (c) Average distance between the center of the NP and the center of mass of the N═N moiety of the *trans* (red) and *cis* (blue) isomer of **A1** as a function of time.

typical experimental situation, and the NP was allowed to equilibrate (20 ns) in a box of water. We found that in their energy-minimized state (Figure 4a, right) these NPs featured *trans*-azobenzene moieties buried within the ligand monolayer; in other words, the high energy of *trans*-**A1** in water was decreased by solvation with long alkyl chains (see also

DOI: 10.1021/jacs.8b09638
J. Am. Chem. Soc. XXXX, XXX, XXX−XXX

Supporting Information, Figure S84). The positively charged ammonium groups of **B1**, on the other hand, retained their initial protruding configuration, which can explain the excellent water solubility of these NPs despite the presence of the hydrophobic *trans*-azobenzene groups.

We separately considered a *cis*-**A1**/**B1**-coated NP (Figure 4b). Similar to their *trans* isomers, the *cis*-azobenzene groups became buried within the nonpolar monolayer, albeit to a lesser (by ∼2 Å) extent, which can be visualized by plotting the average distance of the center of mass of the N═N moiety to the center of the NP (Figure 4c). This result can be rationalized by the more hydrophilic character of the *cis* form, which can interact with water molecules via its nitrogens' lone electron pairs.[50,51] On the basis of these results, we postulate that azobenzene switching in **A1**/**B1**-functionalized NPs occurs within the nonpolar nanoenvironment of the NP-bound alkyl chains[52] (Figure 4, green arrows) rather than in the aqueous phase.

We then proceeded to study azobenzene photoswitching on NPs functionalized with other **A***m*/**B***n* combinations. Both **A2**/**B1**- and **A3**/**B1**-functionalized 2.5 nm NPs behaved analogously to **A1**/**B1** NPs, with the photoisomerization reactions completed within ∼10 min for the *trans* → *cis* and ∼2 min for the *cis* → *trans* reaction, respectively (Supporting Information, Figures S62−S67 and S85). However, increasing the loading of azobenzene on the NPs led to poorer PSSs under the same irradiation conditions (e.g., ∼19% residual *trans*-**A3** for χ = 0.16 **A3**/**B1**-coated NPs, but as much as ∼29% *trans*-**A3** for χ = 0.84 NPs). Interestingly, varying χ had no effect on the kinetics of the back-isomerization reaction: we found that *cis*-**A2** on **A2**/**B1**-coated 2.5 nm NPs relaxed with the same rate constant of $k \approx 0.024$ h^{-1} irrespective of χ (in the range $0.15 \leq \chi \leq 0.49$) (Supporting Information, Figure S68). We were also interested in determining whether the kinetics of thermal relaxation are affected by NP curvature. To this end, we prepared two batches of differently sized Au NPs (2.5 and 5.5 nm) functionalized with mixtures of **A2** and **B2** (χ = 0.13 for 2.5 nm and 0.15 for 5.5 nm) and verified that both could be switched upon UV light irradiation (these studies were performed in a 9:1 (v/v) water−methanol mixture as the solvent; **A2**/**B2**-coated 5.5 nm NPs could not be redispersed in pure water). However, back-isomerization of **A2** on 5.5 nm NPs proceeded markedly (by approximately 2-fold) slower, compared to 2.5 nm NPs (Supporting Information, Figure S69). This result can be explained by the smaller curvature associated with the larger particles,[17,53] which can increase molecular crowding, thus stabilizing the *cis* isomer.

Next, we investigated the effect of ligand length on the switching properties of NP-bound azobenzene. To this end, we functionalized Au NPs with a mixture of a short thiolated-azobenzene **A4** and background ligand **B3** and found that the resulting NPs were readily soluble in water. However, exposure to UV did not induce any changes in the absorption spectra of these NPs, indicating that *trans*-azobenzene groups residing close to the gold surface are difficult to photoisomerize. This can be attributed to the quenching of the excited state of azobenzene by gold, in agreement with previous literature reports.[15,54,55] We therefore considered combining the short background ligand, **B3**, and the long-chain azobenzene, **A1** (Figure 5). Similar to **A1**/**B1**-coated NPs, azobenzene **A1** coadsorbed with **B3** could be readily switched for many cycles, and the reversible isomerization was not accompanied by NP aggregation.

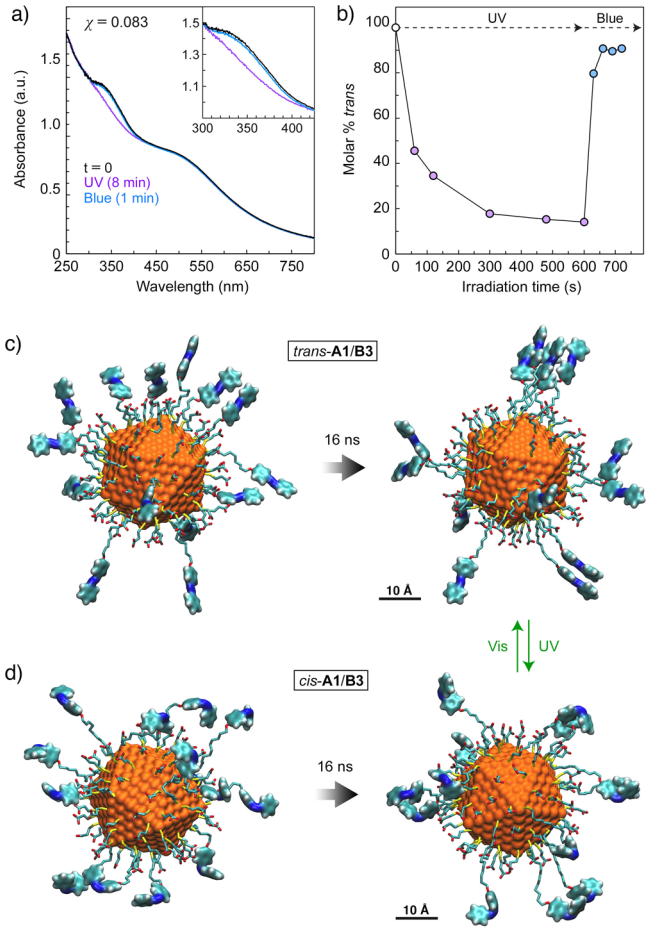

Figure 5. (a) UV/vis absorption spectra of an aqueous solution of **A1**/**B3**-functionalized 2.5 nm Au NPs before (black) and after (purple) exposure to UV light and after subsequent exposure to blue light (in blue). (b) Reversible photoswitching of **A1** on the same NPs. (c, d) Snapshots from MD simulations of an **A1**/**B3**-coated gold NP in the *trans* (c) and *cis* (d) state of azobenzene. The images on the left correspond to t = 0, and those on the right correspond to t = 16 ns.

The good colloidal stability of **A1**/**B3**-functionalized NPs in water may be surprising, given the lack of background ligands' long alkyl chains capable of solvating the azobenzene groups (compare with the right panels of Figure 4a and b). To help explain the efficient hydration of these NPs, we performed additional MD simulations and found that energy-minimized configurations of these NPs in water featured small bundles (aggregates) of azobenzene (Figure 5c,d). As expected, the *trans* isomer of **A1** exhibited a higher propensity to aggregate, with aggregates of up to five azobenzene units, whereas the more polar *cis*-**A1** afforded a ∼1:1 mixture of free and dimerized azobenzenes. These results indicate that in the absence of a nonpolar nanoenvironment on the NP surfaces, the surface energy of the NP−water interface is decreased by stacking the azobenzene units.

Interestingly, we repeatedly observed that the *trans* → *cis* isomerization of azobenzene within the putative bundles on **A1**/**B3**-functionalized NPs proceeds faster (by a factor of ∼2) than on **A1**/**B1**- functionalized NPs at the same value of χ. The seemingly counterintuitive observation that aggregated azobenzenes isomerize faster than isolated ones can be explained by a cooperative switching mechanism, whereby isomerization of an azobenzene unit is facilitated by the switching of its

DOI: 10.1021/jacs.8b09638
J. Am. Chem. Soc. XXXX, XXX, XXX−XXX

neighbor. This mechanism has previously been used to rationalize the accelerated isomerization of azobenzene in the crystalline state[18] and within molecules self-assembled on planar substrates.[16,17,19,20]

Effect of Background Ligand on the Kinetics of Azobenzene Isomerization on Gold Nanoparticles. To investigate the effect of background ligand on the switching properties of azobenzene, we prepared 2.5 nm NPs cofunctionalized with **A2** and several different background ligands (all NPs were at $\chi \approx 0.15$). We found that shortening the alkyl chain of **B1** by five methylene groups (i.e., ligand **B4**) had no effect on the kinetics of the back-isomerization reaction (Figure 6a; $k \approx 0.024$ h^{-1}). Likewise, replacing the terminal positively charged group of **B1** with the negatively charged carboxylate (ligand **B5**) had little effect ($k \approx 0.030$ h^{-1}). In contrast, replacing **B1**'s alkyl chain with a tris(ethylene glycol) chain of similar overall length (**B6**) increased the rate of relaxation approximately 2-fold ($k \approx 0.053$ h^{-1}). We hypothesized that this increase might be related to the high flexibility of OEG chains[56−61] (compared to alkyl chains), resulting in more conformational freedom available to the terminal azobenzene groups. Indeed, analysis of MD simulations of **A2**/**B1**- and **A2**/**B6**-coated NPs (Figures S87−S89 in the Supporting Information) confirmed that when coadsorbed with **B6**, the azobenzene group of **A2** has more conformational freedom. Furthermore, additional acceleration was observed for ligands incorporating longer OEG linkers; see the combinations **A5**/**B7** and **A5**/**B9** below.

Interestingly, when hydroxy-terminated thiol **B8** was used as the background ligand, a dramatic acceleration of azobenzene back-isomerization was observed ($k \approx 4.17$ h^{-1}, corresponding to the thermal half-life of *cis*-azobenzene, $\tau_{1/2}$, of only ∼10 min). We attribute this result to the hydrogen bond (H-bond) formation between **B8**'s OH group and *cis*-**A2**'s nitrogen atoms, which can decrease the double-bond character of the N═N moiety, thereby facilitating the rotation about this bond and reducing the energy barrier to the more stable *trans* isomer (see Figure 6b).

It is interesting to point out an analogy to the study by Tamaoki and co-workers, who synthesized a small-molecule azobenzene appended with a strategically placed phosphate group capable of forming a hydrogen bond with azobenzene's nitrogen.[62] At pH = 7.3, the phosphate group was predominantly deprotonated and *cis*-azobenzene was found to back-isomerize relatively slowly. However, decreasing the solution pH to 6.1 activated H-bonding between *cis*-azobenzene and protonated phosphate, increasing the rate of relaxation by approximately 40-fold.[62]

Hecht et al. has recently shown that azobenzene back-isomerization can be efficiently catalyzed[63,64] by electrons and holes, which, in our case, could potentially originate from the metallic core of the nanoparticle. In fact, the groups of Scaiano,[65] Santer,[66] and Aramendía[67] have demonstrated the fast back-isomerization of azobenzene in proximity to weakly stabilized ("bare") gold NPs. We wish to emphasize, however, that this pathway is unlikely in our case, since (i) the particles are passivated with a protective layer of thiols and, more importantly, (ii) rate acceleration is only observed in the presence of background ligands terminated with hydroxy groups.

To verify the critical role of the hydroxy group, we also prepared NPs cofunctionalized with **A2** + **B2** and found that the rate of thermal relaxation was even faster, $k \approx 10.8$ h^{-1} (Figure 6a). This can be explained by the higher propensity for H-bond formation between **A2** (where the distance between the S atom and the center of mass of the N═N moiety is d_{S-N} = 21.1 Å) and **B2** (the distance between the S and terminal O atoms is d_{S-O} = 20.1 Å; $\Delta d_{A2/B2}$ = 1.0 Å) than between **A2** and **B8** (d_{S-O} = 26.7 Å, $\Delta d_{A2/B8}$ = 5.6 Å; all distances were calculated for extended structures using GaussView software[68]). Overall, our results show that the rate of azobenzene back-isomerization in water can be tuned by a factor of ∼500 simply by changing the background ligand with which it is coadsorbed on gold NPs.

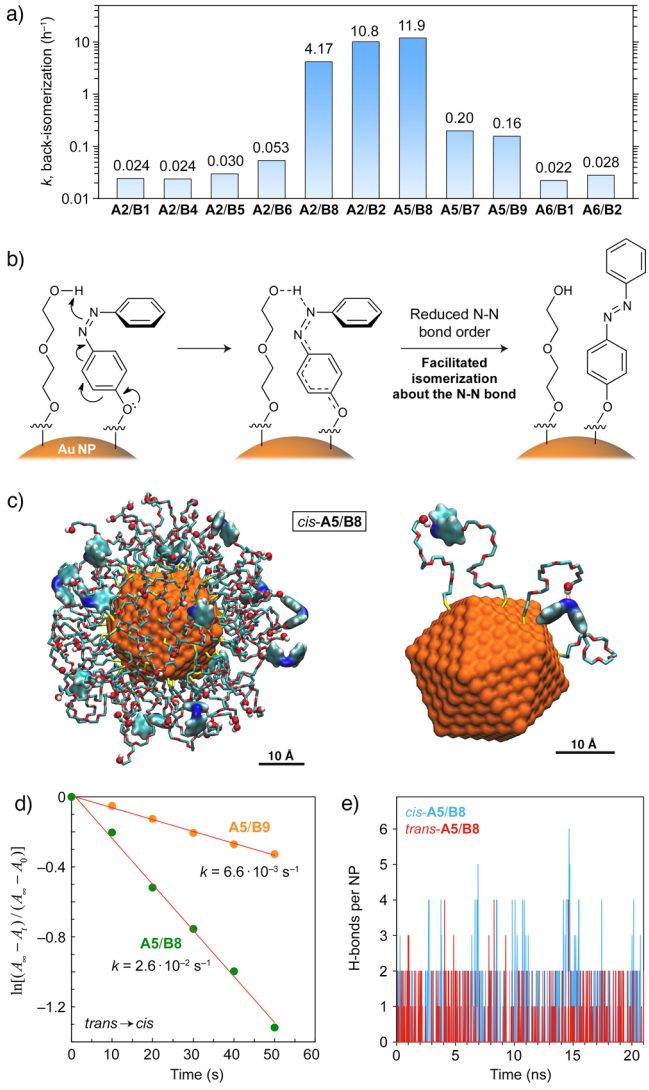

Figure 6. (a) Dependence of the thermal back-isomerization of *cis*-**A2** and *cis*-**A5** on 2.5 nm Au NPs as a function of background ligand **B***n* (note the logarithmic scale). The surface coverage of azobenzene, χ, corresponded to ∼0.15 for all NPs. (b) Proposed mechanism for back-isomerization of *cis*-azobenzene assisted by a neighboring hydroxy group. (c) Snapshots from MD simulations of a *cis*-**A5**/**B8**-coated 2.5 nm gold NP. (d) Differing kinetics of UV-induced *trans* → *cis* azobenzene isomerization on **A5**/**B8**- and **A5**/**B9**-coated 2.5 nm Au NPs ($\chi \approx 0.15$ in both cases) (here, A_0 is the initial absorbance at ∼350 nm, A_t is the absorbance after exposure to UV light for time t, and A_∞ is the absorbance after exhaustive exposure to UV (PSS)[69]). (e) Number of hydrogen bonds (by MD simulations) between **B8** and *trans*- vs *cis*-**A5** over a period of ∼20 ns.

DOI: 10.1021/jacs.8b09638
J. Am. Chem. Soc. XXXX, XXX, XXX−XXX

Extending the OEG chain of **A2** by three EG units (i.e., ligand **A5**) again resulted in a fast back-isomerization reaction ($k \approx 11.9$ h^{-1} on **A5**/**B8**-functionalized 2.5 nm NPs, corresponding to a $\tau_{1/2}$ value of 3.5 min). Although this result may appear surprising given the relatively large $\Delta d_{A5/B8} = 5.5$ Å (d_{S-N} in **A5** = 32.2 Å), it can be explained by the high flexibility of long OEG chains, which can facilitate interactions between H-bond donors and acceptors. When, however, the distance between the donor and acceptor sites was increased to $\Delta d = 16.3$ Å (using the **A5** + **B7** combination; d_{S-O} in **B7** = 15.9 Å), the rate of back-isomerization dropped substantially ($k \approx 0.20$ h^{-1}; see Figure 6a).

An ideal control experiment verifying the importance of hydrogen bonding between coadsorbed azobenzene- and hydroxy-terminated thiols would be based on replacing the acidic hydrogen with a methyl group. To this end, we synthesized ligand **B9** and indeed found that the rate of back-isomerization decreased from 11.9 h^{-1} (for **A5**/**B8**) to 0.16 h^{-1} (**A5**/**B9**). This on-nanoparticle H-bonding was further investigated by MD simulations, which revealed the presence of H-bonds between *cis*-**A5** and **B8** residing on the same NPs (Figure 6c). In sharp contrast, the terminal methoxy groups of **B9** were exposed to the solvent; see Supporting Information, Figure S91a.

We separately simulated a mixture of *trans*-**A5** and **B8** coadsorbed on 2.5 nm Au NPs. These simulations showed that the *trans* isomer of **A5** may also be capable of forming H-bonds with **B8**'s hydroxy group (Supporting Information, Figure S91b), thus possibly reducing the double-bond character of the N═N group and increasing the rate of the *trans* → *cis* forward-isomerization. To verify this hypothesis, we exposed NPs functionalized with *trans*-**A5**/**B8** and *trans*-**A5**/**B9** to UV light for increasing periods and found that, indeed, isomerization proceeded faster with the OH-terminated **B8** as the background ligand (Figure 6d). The difference in rates, however, was much smaller than in the case of back-isomerization (~4 and ~74, respectively), which can be accounted for by the lower percentage of *trans*-**A5** vs *cis*-**A5** engaged in H-bonding with **B8** (estimated as 0.7% and 1.9%, respectively, over a period of of 20 ns; Figure 6e) and by the lower strength of H-bonds formed by *trans*-**A5** (a significant distortion from planarity in the O–H···N moiety; see Figure S91c in the Supporting Information).

To verify the mechanism shown in Figure 6b (specifically, the importance of the oxygen atom at the *para* position of azobenzene), we also synthesized thiolated azobenzene **A6** with an alkyl—as opposed to alkoxy—substituent at the *para* position. Interestingly, this small change in the structure of azobenzene had a profound effect on the kinetics of back-isomerization, with nearly no acceleration observed in the presence of hydroxy-terminated background ligand **B2** (compare $k \approx 0.028$ h^{-1} for **A6**/**B2**-coated NPs with $k \approx 10.8$ h^{-1} for **A2**/**B2**-coated NPs; Supporting Information, Figures S71 and S73). These results are in agreement with our earlier results on light-induced self-assembly of NPs in nonpolar solvents, where we showed that the surface polarity of NPs coated with 4,4′-dialkoxysubstituted *cis*-azobenzenes is much higher compared to NPs functionalized with *cis*-azobenzenes having only one substituent at the *para* position.[13,70] In other words, removing the electron-donating alkoxy substituent in **A6** decreased the electron density on the nitrogen atoms, thus decreasing the hydrogen-bond-accepting character of the *cis*-azobenzene group.

Next, we investigated the effect of solvent on the intermolecular interactions between azobenzene **A5** and background ligands. To this end, we prepared concentrated solutions of **A5**/**B8**-functionalized 2.5 nm Au NPs in water and diluted them with 24 volumes of various organic solvents (i.e., volume fractions of water in the resulting solutions = 4%). We hypothesized that organic solvents can solvate azobenzene and/or hydroxy groups, thus weakening the H-bonding between them. Indeed, the presence of organic solvents decreased the rate of thermal relaxation of *cis*-**A5** from $k \approx 11.9$ h^{-1} (pure water) all the way to $k \approx 0.025$ h^{-1} (for 24:1 dioxane–water) (Figure 7a; see also Supporting Information, Figure S74). Notably, the back-isomerization rates in DMF-, acetone-, and dioxane-rich solutions were similar to those of free **A5** in organic solvents, suggesting excellent solvation of

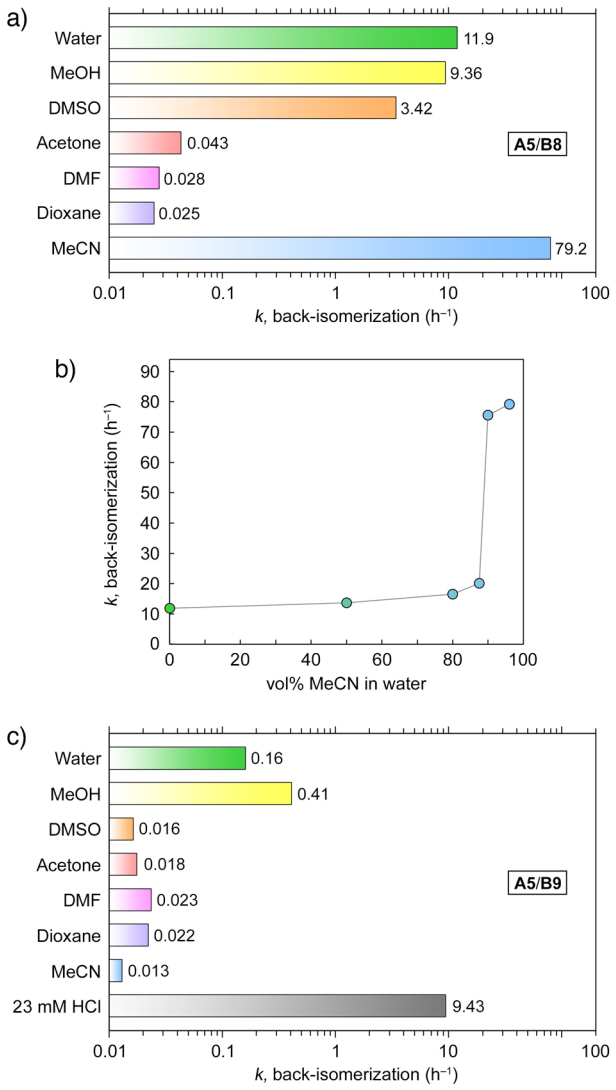

Figure 7. (a) Rates of thermal back-isomerization of *cis*-**A5** on **A5**/**B8**-functionalized 2.5 nm Au NPs in different 1:24 water–solvent mixtures, where the solvent is indicated on the left. (b) Dependence of the back-isomerization rate of *cis*-**A5** on **A5**/**B8**-functionalized 2.5 nm Au NPs as a function of the composition of the acetonitrile–water mixture. (c) Rates of the thermal back-isomerization of *cis*-**A5** on **A5**/**B9**-functionalized 2.5 nm Au NPs in different 1:24 water–solvent mixtures, where the solvent is indicated on the left (HCl solution in pure water).

DOI: 10.1021/jacs.8b09638
J. Am. Chem. Soc. XXXX, XXX, XXX–XXX

the terminal groups of **A5** and **B8** and no strong interactions between them. Surprisingly, however, the addition of acetonitrile (MeCN) led to a pronounced increase in the reaction rate ($k \approx 79.2$ h^{-1}), indicating efficient stabilization of the intermolecular interactions between **A5** and **B8** in this solvent. To confirm that the >3000-fold difference (0.025 h^{-1} vs 79.2 h^{-1}) in relaxation kinetics in dioxane- and MeCN-rich solutions is due to intermolecular interactions on NPs and interactions of azobenzene with solvent molecules, we prepared solutions of small-molecule **A5** in dioxane and MeCN and found only a small (~1.2-fold) difference in the back-isomerization rates (Supporting Information, Figure S72). By studying the behavior of **A5**/**B8**-functionalized NPs in several different MeCN–water mixtures, we found that the transition between the fast and the very fast regime occurs between 87.5% and 90% v/v MeCN contents (Figure 7b; see also Supporting Information, Figure S75). We therefore speculate that when present at ≥10%, water can to some extent interfere with the on-NP H-bond formation; however at ≤7.5%, no such competition exists.

As expected, replacing **B8**'s OH group with OMe decreased the kinetics of back-isomerization in all solvents (Figure 7c). The extent of decrease was most striking for the 24:1 MeCN–water mixture, where the relaxation rate of *cis*-**A5** decreased by a factor of ~6100 simply by replacing background ligand **B8** with **B9** (as illustrated in the abstract graphic). We also studied the back-isomerization of *cis*-**A5** coadsorbed with **B9** in the presence of a strong acid, potentially capable of reducing the bond order of the N═N moiety, thus facilitating back-isomerization. Indeed, reducing a solution's pH from 7 to ~1.6 increases the rate from ~0.16 h^{-1} to ~9.43 h^{-1} (23 mM HCl in Figure 7c). Quite remarkably, $k \approx 9.43$ h^{-1}, observed for **A5**/**B9**-functionalized NPs at a low pH, was still lower than $k \approx 11.9$ h^{-1} found for **A5**/**B8**-coated NPs at pH = 7, emphasizing the importance of preorganization/high effective molarity on hydrogen bond formation.

Having discussed the properties of azobenzenes on the surfaces of water-soluble NPs, we revisit the issue of ligand mixing on NP surfaces. We argue that, with the exception of NPs decorated with the very short background ligand **B3** (Figure 5c,d), thiolated azobenzenes **A*m*** and background ligands **B*n*** are intermixed and do not phase-separate on NPs. This argument is supported by the following observations. First, NPs featuring patches of azobenzene would have a propensity to aggregate into small clusters by hydrophobic interactions; no such clusters could be detected by TEM. Second, replacing the background ligand on azobenzene-coated NPs would have little effect on the switching properties of azobenzenes if **A*m*** and **B*n*** were phase-separated; however, we found that the properties of azobenzene are greatly affected by the background ligand. In particular, all the azobenzene units on NPs cofunctionalized with **A*m*** and hydroxy-terminated background ligands back-isomerize rapidly, suggesting that each has at least one OH-donating neighbor. Third, the back-isomerization rate was independent of χ, as demonstrated for **A2**/**B1**-functionalized 2.5 nm gold NPs, suggesting that a good mixing of the two ligands exists. It is important to point out that the first step of our ligand-exchange protocol (i.e., treating DDA-coated NPs with a substoichiometric amount of azobenzene) most likely does lead to patches of azobenzene; it is the subsequent addition of an excess of thiols that apparently results in equilibration to monolayers of intermixed ligands.

Accelerated Back-Isomerization of Azobenzene on Other Inorganic Nanoparticles. To further confirm that the accelerated relaxation of *cis*-azobenzene on NPs is not induced by the plasmonic nature of gold particles, we coadsorbed azobenzene-terminated ligands with hydroxy-terminated background ligands on other inorganic NPs. First, we prepared water-soluble 3.5 nm palladium NPs cofunctionalized with **A2** and **B2** (Figure 8 and Supporting Information, Section 8) and

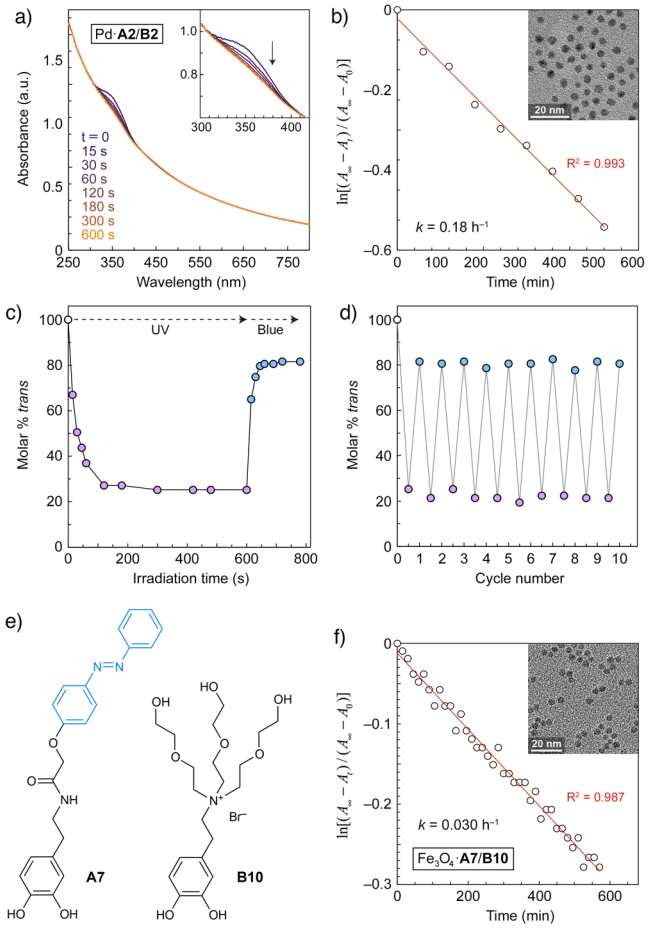

Figure 8. (a) Evolution of the UV/vis absorption spectra of an aqueous solution of **A2**/**B2**-functionalized 3.5 nm Pd NPs ($\chi \approx 0.10$) under UV light exposure. (b) Kinetics of the thermal back-isomerization of **A2** on these NPs. The inset shows a representative TEM image of water-soluble **A2**/**B2**-functionalized 3.5 nm Pd NPs. (c) Reversible photoswitching of **A2** on **A2**/**B2**-functionalized 3.5 nm Pd NPs. (d) Reversible switching of azobenzene for 10 cycles (5 min of UV and 2 min of blue light irradiation were applied in each cycle). (e) Structural formulas of catechol-based ligands for Fe_3O_4 NPs: azobenzene-terminated ligand **A7** and hydroxy-terminated ligand **B10**. (f) Kinetics of the thermal back-isomerization of **A7** on **A7**/**B10**-functionalized 4.0 nm Fe_3O_4 NPs ($\chi \approx 0.10$). The inset shows a representative TEM image of these NPs.

verified that **A2** could be reversibly isomerized on these NPs (Figure 8a–d). Although a significant (~11-fold) acceleration was observed ($k \approx 0.18$ h^{-1}, compared with $k \approx 0.016$ h^{-1} for small-molecule **A2** in DMSO), the effect was much less pronounced than on **A2**/**B2**-coated 2.5 nm Au NPs ($k \approx 10.8$ h^{-1}, i.e., ~700-fold acceleration), which could be due to the previously reported oxidation of the Pd NP surface (to PdO), which decreases the overall density of thiolate ligands on these

DOI: 10.1021/jacs.8b09638
J. Am. Chem. Soc. XXXX, XXX, XXX–XXX

NPs, thereby increasing the average distance between hydrogen bond donors (OH groups) and acceptors (azobenzene).[71]

We also synthesized 4.0 nm Fe_3O_4 (magnetite) NPs cofunctionalized with the previously reported[45] azobenzene **A7** and hydroxy-terminated background ligand **B10** (Figure 8e). Despite considering several hydroxy-terminated background ligands, we did not succeed in preparing water-soluble, azobenzene-coated Fe_3O_4 NPs and studied their properties in 2:1 v/v toluene−methanol. Azobenzene **A7** on these NPs back-isomerized with $k \approx 0.030\ h^{-1}$ (Figure 8f), corresponding to a minor acceleration effect (~3-fold; $k \approx 0.0097\ h^{-1}$ for free **A7** in the same solvent mixture; Supporting Information, Figure S78), which could be attributed to the relatively large footprint of catechol-based ligands[45,72] and consequently decreased intermolecular interactions between **A7** and **B10**. Nevertheless, the accelerated reaction on both Pd and Fe_3O_4 NPs, together with the other experimental observations and computer simulations, indicate that fast thermal relaxation of *cis*-azobenzene on nanoparticulate platforms is predominantly (if not exclusively) due to intermolecular coupling to the nearby hydroxy-terminated ligands.

Wetting Properties of Aqueous Solutions of Azobenzene-Functionalized Nanoparticles. Finally, we were interested in determining whether azobenzene switching on NPs could affect the properties of the aqueous solutions of these particles. To this end, we placed 10 μL water droplets containing increasing amounts of **A2**/**B1**-functionalized 2.5 nm Au NPs ($\chi \approx 0.53$) on top of polystyrene (PS) Petri dishes and determined the contact angles as a function of NP concentration (Figure 9a, red markers). We found that the contact angle, $\angle$, decreased from ~90° (pure water) to 55 ± 3° even for a dilute ($c = 0.10\ \mu M$) aqueous solution of these NPs. For concentrations ≥ 0.83 μM, the droplets were found to wet the surface completely (superwetting regime, $\angle \approx 0°$; Figure 9b, second from the left). These results suggest that azobenzenes bound to one hemisphere of each NP interact with the hydrophobic PS surface, whereas azobenzenes on the other hemisphere remain buried inside the mixed monolayer, facilitating hydration and efficient wetting of PS substrates; in other words, these NPs can act as "nanoscale surfactants". Indeed, decreasing the fractional coverage of **A2** required higher concentrations of NPs to achieve wetting of PS: the contact angle of $\chi \approx 0.33$ NPs dropped below 60° only when a $c = 5.8\ \mu M$ solution was used, whereas aqueous solutions of $\chi \approx 0.15$ NPs did not spread on PS even at a high ($c = 11.6\ \mu M$) concentration of NPs (Figure 9a, green and red markers, respectively).

When the solution of $\chi \approx 0.53$, **A2**/**B1**-functionalized 2.5 nm Au NPs were exposed to 10 min of UV light (resulting in PSS containing ~31% of residual *trans*) prior to being deposited on the PS substrate, wetting was suppressed ($\angle \approx 29°$; Figure 9b, the third from the left). This effect was observed for a wide range of NP concentrations ($0.1\ \mu M \le c \le 2.9\ \mu M$; purple markers in Figure 9a) and could be explained by the higher affinity of the *trans* isomer of **A2** (compared with the more hydrophilic *cis*-**A2**) to the underlying PS surface. Pre-exposing the same NP solution to 10 min of UV and then to 2 min of blue light produced a PSS comprising ~93% *trans*-**A2**, resulting in the complete wetting of PS (Figure 9b, right). Interestingly, placing the same NP solution onto a more hydrophilic surface (we worked with silicon wafers) had the opposite effect: we found that pre-exposure to UV light facilitated spreading (Figure 9c), which could be attributed to the favorable interactions[50,51] between the *cis*-azobenzene moieties and the surface OH groups.

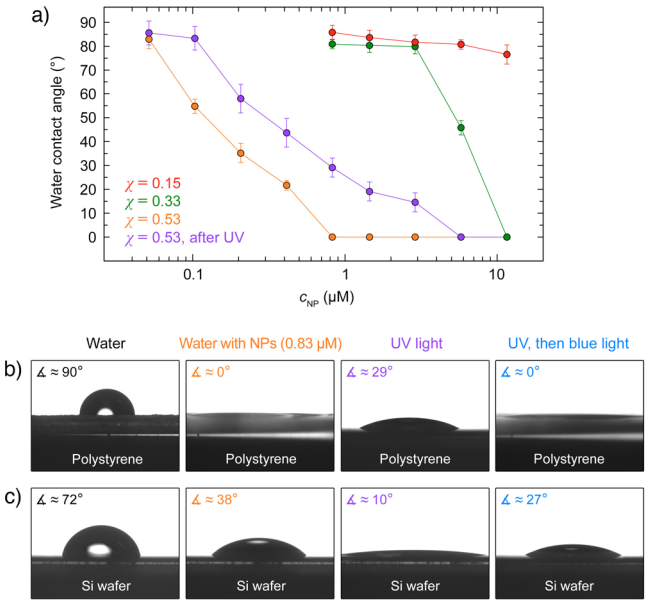

Figure 9. (a) Contact angles of aqueous solutions of **A2**/**B1**-functionalized 2.5 nm Au NPs on polystyrene as a function of the fractional coverage of azobenzene on the NPs (χ). (b, c) Photographs of water droplets (left) and droplets of a 0.83 μM aqueous solution of $\chi = 0.53$ NPs placed on polystyrene (b) and silicon wafer (c) before and after exposure to light.

CONCLUSIONS

In sum, we co-deposited several thiolated azobenzenes with thiols terminated with various polar functional groups on the surfaces of gold nanoparticles. Owing to the polar nature of the latter, "background" ligands, the resulting NPs were readily soluble in different polar solvents, including water. Depending on the length of the background ligand, the intrinsically hydrophobic azobenzene groups self-organized into two distinct supramolecular architectures, identified with the help of molecular dynamics simulations. Azobenzene adsorbed on NP surfaces retained its light-switchable properties and, once isomerized to the *cis* isomer, spontaneously back-isomerized in a reaction that obeyed first-order kinetics. These NPs allowed us to systematically investigate the kinetics of azobenzene back-isomerization as a function of the background ligand. In the course of these studies, we found that background ligands terminated with the hydroxy group increased the rate of back-isomerization. We demonstrated that simply replacing the terminal methoxy group with an OH could facilitate the reaction by a factor of >6000. Efficient acceleration was observed only in cases where the length of the background ligand was similar to that of the azobenzene-terminated thiol, suggesting the involvement of intermolecular interactions (hydrogen bonding) between the two species. Several groups have previously reported on the fast thermal relaxation of *cis*-azobenzenes bearing hydroxy substituents at the *para* position.[73−76] In all these cases, however, the acceleration was attributed to the ability of these azophenols to undergo partial deprotonation. We showed that nanoparticle surfaces provide an environment that promotes intermolecular interactions, resulting in unprecedented rates of back-isomer-

DOI: 10.1021/jacs.8b09638
J. Am. Chem. Soc. XXXX, XXX, XXX−XXX

ization even in azobenzenes lacking the hydroxy group. Our results pave the way toward the development of novel light-responsive materials operating in aqueous media and, in the long run, in biological environments. Importantly, these studies can readily be extended to other switchable molecules[77−79] and background ligands, as well as to nanoparticles of other sizes and compositions, including upconversion NPs.[80]

■ ASSOCIATED CONTENT

Supporting Information

The Supporting Information is available free of charge on the ACS Publications website at DOI: 10.1021/jacs.8b09638.

Figures S1−S92; Schemes S1−S9; detailed description of the synthesis and analysis of ligands, preparation, functionalization, and analysis of nanoparticles, molecular dynamics simulations; description of supporting movies; supporting references (PDF)

Movie (MPG)

Movie (MPG)

Movie (MPG)

Movie (MPG)

■ AUTHOR INFORMATION

Corresponding Author

*rafal.klajn@weizmann.ac.il

ORCID

Soumen De: 0000-0003-4674-9183

Petr Král: 0000-0003-2992-9027

Rafal Klajn: 0000-0002-6320-8875

Notes

The authors declare no competing financial interest.

■ ACKNOWLEDGMENTS

This work was supported by the European Research Council (grant #336080 to R.K.), the Israel Ministry of Science (China−Israel cooperation, grant 3-13555 to R.K.), and the NSF (Division of Materials Research, grant #1506886 to P.K.). Z.C. acknowledges support from the Planning and Budgeting Committee of the Council for Higher Education, the Koshland Foundation, and a McDonald−Leapman grant. Anton I. Hanopolskyi is acknowledged for donating crude compound **22**.

■ REFERENCES

(1) Hartley, G. S. The *Cis*-Form of Azobenzene. *Nature* **1937**, *140*, 281.

(2) Peters, M. V.; Stoll, R. S.; Kühn, A.; Hecht, S. Photoswitching of Basicity. *Angew. Chem., Int. Ed.* **2008**, *47*, 5968−5972.

(3) Imahori, T.; Yamaguchi, R.; Kurihara, S. Azobenzene-Tethered Bis(Trityl Alcohol) as a Photoswitchable Cooperative Acid Catalyst for Morita-Baylis-Hillman Reactions. *Chem. - Eur. J.* **2012**, *18*, 10802−10807.

(4) Osorio-Planes, L.; Rodríguez-Escrich, C.; Pericàs, M. A. Photoswitchable Thioureas for the External Manipulation of Catalytic Activity. *Org. Lett.* **2014**, *16*, 1704−1707.

(5) Shinkai, S.; Minami, T.; Kusano, Y.; Manabe, O. Photoresponsive Crown Ether. 2. Photocontrol of Ion Extraction and Ion Transport by a Bis(crown Ether) with a Butterfly-Like Motion. *J. Am. Chem. Soc.* **1983**, *105*, 1851−1856.

(6) Laprell, L.; Repak, E.; Franckevicius, V.; Hartrampf, F.; Terhag, J.; Hollmann, M.; Sumser, M.; Rebola, N.; DiGregorio, D. A.; Trauner, D. Optical Control of NMDA Receptors with a Diffusible Photoswitch. *Nat. Commun.* **2015**, *6*, 8076.

(7) Velema, W. A.; van der Berg, J. P.; Hansen, M. J.; Szymanski, W.; Driessen, A. J. M.; Feringa, B. L. Optical Control of Antibacterial Activity. *Nat. Chem.* **2013**, *5*, 924−928.

(8) Muraoka, T.; Kinbara, K.; Aida, T. Mechanical Twisting of a Guest by a Photoresponsive Host. *Nature* **2006**, *440*, 512−515.

(9) Jaschke, M.; Schonherr, H.; Wolf, H.; Butt, H. J.; Bamberg, E.; Besocke, M. K.; Ringsdorf, H. Structure of Alkyl and Perfluoroalkyl Disulfide and Azobenzenethiol Monolayers on Gold(111) Revealed by Atomic Force Microscopy. *J. Phys. Chem.* **1996**, *100*, 2290−2301.

(10) Yu, H. Z.; Wang, Y. Q.; Cheng, J. Z.; Zhao, J. W.; Cai, S. M.; Inokuchi, H.; Fujishima, A.; Liu, Z. F. Electrochemical Behavior of Azobenzene Self-Assembled Monolayers on Gold. *Langmuir* **1996**, *12*, 2843−2848.

(11) Wang, R.; Iyoda, T.; Jiang, L.; Tryk, D. A.; Hashimoto, K.; Fujishima, A. Structural Investigation of Azobenzene-Containing Self-Assembled Monolayer Films. *J. Electroanal. Chem.* **1997**, *438*, 213−219.

(12) Kondo, T.; Kanai, T.; Uosaki, K. Control of the Charge-Transfer Rate at a Gold Electrode Modified with a Self-Assembled Monolayer Containing Ferrocene and Azobenzene by Electro- and Photochemical Structural Conversion of Cis and Trans Forms of the Azobenzene Moiety. *Langmuir* **2001**, *17*, 6317−6324.

(13) Klajn, R.; Bishop, K. J. M.; Grzybowski, B. A. Light-Controlled Self-Assembly of Reversible and Irreversible Nanoparticle Suprastructures. *Proc. Natl. Acad. Sci. U. S. A.* **2007**, *104*, 10305−10309.

(14) Samanta, D.; Gemen, J.; Chu, Z.; Diskin-Posner, Y.; Shimon, L. J. W.; Klajn, R. Reversible Photochromism of Encapsulated Azobenzenes in Water. *Proc. Natl. Acad. Sci. U. S. A.* **2018**, *115*, 9379−9384.

(15) Klajn, R. Immobilized Azobenzenes for the Construction of Photoresponsive Materials. *Pure Appl. Chem.* **2010**, *82*, 2247−2279.

(16) Pace, G.; Ferri, V.; Grave, C.; Elbing, M.; von Hänisch, C.; Zharnikov, M.; Mayor, M.; Rampi, M. A.; Samorì, P. Cooperative Light-Induced Molecular Movements of Highly Ordered Azobenzene Self-Assembled Monolayers. *Proc. Natl. Acad. Sci. U. S. A.* **2007**, *104*, 9937−9942.

(17) Moldt, T.; Brete, D.; Przyrembel, D.; Das, S.; Goldman, J. R.; Kundu, P. K.; Gahl, C.; Klajn, R.; Weinelt, M. Tailoring the Properties of Surface-Immobilized Azobenzenes by Monolayer Dilution and Surface Curvature. *Langmuir* **2015**, *31*, 1048−1057.

(18) Lai, C. Y.; Raj, G.; Liepuoniute, I.; Chiesa, M.; Naumov, P. Direct Observation of Photoinduced *Trans-Cis* Isomerization on Azobenzene Single Crystal. *Cryst. Growth Des.* **2017**, *17*, 3306−3312.

(19) Zheng, Y. B.; Pathem, B. K.; Hohman, J. N.; Thomas, J. C.; Kim, M.; Weiss, P. S. Photoresponsive Molecules in Well-Defined Nanoscale Environments. *Adv. Mater.* **2013**, *25*, 302−312.

(20) Pathem, B. K.; Claridge, S. A.; Zheng, Y. B.; Weiss, P. S. Molecular Switches and Motors on Surfaces. *Annu. Rev. Phys. Chem.* **2013**, *64*, 605−630.

(21) Hostetler, M. J.; Templeton, A. C.; Murray, R. W. Dynamics of Place-Exchange Reactions on Monolayer-Protected Gold Cluster Molecules. *Langmuir* **1999**, *15*, 3782−3789.

(22) Liu, X.; Yu, M.; Kim, H.; Mameli, M.; Stellacci, F. Determination of Monolayer-Protected Gold Nanoparticle Ligand-Shell Morphology using NMR. *Nat. Commun.* **2012**, *3*, 1182.

(23) Kay, E. R. Dynamic Covalent Nanoparticle Building Blocks. *Chem. - Eur. J.* **2016**, *22*, 10706−10716.

(24) Yang, Y.; Serrano, L. A.; Guldin, S. A. Versatile AuNP Synthetic Platform for Decoupled Control of Size and Surface Composition. *Langmuir* **2018**, *34*, 6820−6826.

(25) Chu, Z. L.; Han, Y. X.; Kral, P.; Klajn, R. "Precipitation on Nanoparticles": Attractive Intermolecular Interactions Stabilize Specific Ligand Ratios on the Surfaces of Nanoparticles. *Angew. Chem., Int. Ed.* **2018**, *57*, 7023−7027.

(26) Edwards, W.; Marro, N.; Turner, G.; Kay, E. R. Continuum Tuning of Nanoparticle Interfacial Properties by Dynamic Covalent Exchange. *Chem. Sci.* **2018**, *9*, 125−133.

(27) Klajn, R.; Fang, L.; Coskun, A.; Olson, M. A.; Wesson, P. J.; Stoddart, J. F.; Grzybowski, B. A. Metal Nanoparticles Functionalized

DOI: 10.1021/jacs.8b09638
J. Am. Chem. Soc. XXXX, XXX, XXX−XXX

with Molecular and Supramolecular Switches. *J. Am. Chem. Soc.* **2009**, *131*, 4233−4235.
(28) Manna, A.; Chen, P. L.; Akiyama, H.; Wei, T. X.; Tamada, K.; Knoll, W. Optimized Photoisomerization on Gold Nanoparticles Capped by Unsymmetrical Azobenzene Disulfides. *Chem. Mater.* **2003**, *15*, 20−28.
(29) Raimondo, C.; Reinders, F.; Soydaner, U.; Mayor, M.; Samorì, P. Light-Responsive Reversible Solvation and Precipitation of Gold Nanoparticles. *Chem. Commun.* **2010**, *46*, 1147−1149.
(30) Chovnik, O.; Balgley, R.; Goldman, J. R.; Klajn, R. Dynamically Self-Assembling Carriers Enable Guiding of Diamagnetic Particles by Weak Magnets. *J. Am. Chem. Soc.* **2012**, *134*, 19564−19567.
(31) Köhntopp, A.; Dabrowski, A.; Malicki, M.; Temps, F. Photoisomerisation and Ligand-Controlled Reversible Aggregation of Azobenzene-Functionalised Gold Nanoparticles. *Chem. Commun.* **2014**, *50*, 10105−10107.
(32) Lee, J.-W.; Klajn, R. Dual-Responsive Nanoparticles that Aggregate under the Simultaneous Action of Light and CO_2. *Chem. Commun.* **2015**, *51*, 2036−2039.
(33) Velema, W. A.; Szymanski, W.; Feringa, B. L. Photopharmacology: Beyond Proof of Principle. *J. Am. Chem. Soc.* **2014**, *136*, 2178−2191.
(34) Broichhagen, J.; Frank, J. A.; Trauner, D. A Roadmap to Success in Photopharmacology. *Acc. Chem. Res.* **2015**, *48*, 1947−1960.
(35) Bidoggia, S.; Milocco, F.; Polizzi, S.; Canton, P.; Saccani, A.; Sanavio, B.; Krol, S.; Stellacci, F.; Pengo, P.; Pasquato, L. Fluorinated and Charged Hydrogenated Alkanethiolates Grafted on Gold: Expanding the Diversity of Mixed-Monolayer Nanoparticles for Biological Applications. *Bioconjugate Chem.* **2017**, *28*, 43−52.
(36) Kalsin, A. M.; Kowalczyk, B.; Wesson, P.; Paszewski, M.; Grzybowski, B. A. Studying the Thermodynamics of Surface Reactions on Nanoparticles by Electrostatic Titrations. *J. Am. Chem. Soc.* **2007**, *129*, 6664−6665.
(37) Gao, J. H.; Zhang, O.; Ren, J.; Wu, C. L.; Zhao, Y. B. Aromaticity/Bulkiness of Surface Ligands to Promote the Interaction of Anionic Amphiphilic Gold Nanoparticles with Lipid Bilayers. *Langmuir* **2016**, *32*, 1601−1610.
(38) Rao, A.; Roy, S.; Unnikrishnan, M.; Bhosale, S. S.; Devatha, G.; Pillai, P. P. Regulation of Interparticle Forces Reveals Controlled Aggregation in Charged Nanoparticles. *Chem. Mater.* **2016**, *28*, 2348−2355.
(39) Lee, H. Y.; Shin, S. H. R.; Drews, A. M.; Chirsan, A. M.; Lewis, S. A.; Bishop, K. J. M. *ACS Nano* **2014**, *8*, 9979−9987.
(40) Pillai, P. P.; Kowalczyk, B.; Pudlo, W. J.; Grzybowski, B. A. Electrostatic Titrations Reveal Surface Compositions of Mixed, On-Nanoparticle Monolayers Comprising Positively and Negatively Charged Ligands. *J. Phys. Chem. C* **2016**, *120*, 4139−4144.
(41) Lee, H. Y.; Shin, S. H. R.; Abezgauz, L. L.; Lewis, S. A.; Chirsan, A. M.; Danino, D. D.; Bishop, K. J. M. Integration of Gold Nanoparticles into Bilayer Structures via Adaptive Surface Chemistry. *J. Am. Chem. Soc.* **2013**, *135*, 5950−5953.
(42) Bradford, S. M.; Fisher, E. A.; Meli, M. V. Ligand Shell Composition-Dependent Effects on the Apparent Hydrophobicity and Film Behavior of Gold Nanoparticles at the Air-Water Interface. *Langmuir* **2016**, *32*, 9790−9796.
(43) Strong, L.; Whitesides, G. M. Structures of Self-Assembled Monolayer Films of Organosulfur Compounds Adsorbed on Gold Single Crystals: Electron Diffraction Studies. *Langmuir* **1988**, *4*, 546−558.
(44) Kim, H.; Carney, R. P.; Reguera, J.; Ong, Q. K.; Liu, X.; Stellacci, F. Synthesis and Characterization of Janus Gold Nanoparticles. *Adv. Mater.* **2012**, *24*, 3857−3863.
(45) Das, S.; Ranjan, P.; Maiti, P. S.; Singh, G.; Leitus, G.; Klajn, R. Dual-Responsive Nanoparticles and their Self-Assembly. *Adv. Mater.* **2013**, *25*, 422−426.
(46) Manna, D.; Udayabhaskararao, T.; Zhao, H.; Klajn, R. Orthogonal Light-Induced Self-Assembly of Nanoparticles using Differently Substituted Azobenzenes. *Angew. Chem., Int. Ed.* **2015**, *54*, 12394−12397.
(47) Heaven, M. W.; Dass, A.; White, P. S.; Holt, K. M.; Murray, R. W. Crystal Structure of the Gold Nanoparticle $[N(C_8H_{17})_4][Au_{25}(SCH_2CH_2Ph)_{18}]$. *J. Am. Chem. Soc.* **2008**, *130*, 3754−3755.
(48) Zhu, M.; Lanni, E.; Garg, N.; Bier, M. E.; Jin, R. Kinetically Controlled, High-Yield Synthesis of Au_{25} Clusters. *J. Am. Chem. Soc.* **2008**, *130*, 1138−1139.
(49) Mori, T.; Hegmann, T. Determining the Composition of Gold Nanoparticles: A Compilation of Shapes, Sizes, and Calculations using Geometric Considerations. *J. Nanopart. Res.* **2016**, *18*, 295.
(50) Zhao, H.; Sen, S.; Udayabhaskararao, T.; Sawczyk, M.; Kučanda, K.; Manna, D.; Kundu, P. K.; Lee, J.-W.; Král, P.; Klajn, R. Reversible Trapping and Reaction Acceleration within Dynamically Self-Assembling Nanoflasks. *Nat. Nanotechnol.* **2016**, *11*, 82−88.
(51) Moldt, T.; Przyrembel, D.; Schulze, M.; Bronsch, W.; Boie, L.; Brete, D.; Gahl, C.; Klajn, R.; Tegeder, P.; Weinelt, M. Differing Isomerization Kinetics of Azobenzene-Functionalized Self-Assembled Monolayers in Ambient Air and in Vacuum. *Langmuir* **2016**, *32*, 10795−10801.
(52) Taguchi, T.; Isozaki, K.; Miki, K. Enhanced Catalytic Activity of Self-Assembled-Monolayer-Capped Gold Nanoparticles. *Adv. Mater.* **2012**, *24*, 6462−6467.
(53) Zdobinsky, T.; Maiti, P. S.; Klajn, R. Support Curvature and Conformational Freedom Control Chemical Reactivity of Immobilized Species. *J. Am. Chem. Soc.* **2014**, *136*, 2711−2714.
(54) Zhang, J.; Whitesell, J. K.; Fox, M. A. Photoreactivity of Self-Assembled Monolayers of Azobenzene or Stilbene Derivatives Capped on Colloidal Gold Clusters. *Chem. Mater.* **2001**, *13*, 2323−2331.
(55) Thomas, K. G.; Kamat, P. V. Chromophore-Functionalized Gold Nanoparticles. *Acc. Chem. Res.* **2003**, *36*, 888−898.
(56) Ahmed, S. A.; Tanaka, M. Synthesis of Oligo(ethylene glycol) toward 44-mer. *J. Org. Chem.* **2006**, *71*, 9884−9886.
(57) Han, J.-M.; Pan, J.-L.; Lei, T.; Liu, C.; Pei, J. Smart Macrocyclic Molecules: Induced Fit and Ultrafast Self-Sorting Inclusion Behavior through Dynamic Covalent Chemistry. *Chem. - Eur. J.* **2010**, *16*, 13850−13861.
(58) Prest, P.-J.; Prince, R. B.; Moore, J. S. Supramolecular Organization of Oligo(m-phenylene ethynylene)s in the Solid-State. *J. Am. Chem. Soc.* **1999**, *121*, 5933−5939.
(59) Aykaç, A.; Martos-Maldonado, M. C.; Casas-Solvas, J. M.; Quesada-Soriano, I.; García-Maroto, F.; García-Fuentes, L.; Vargas-Berenguel, A. β-Cyclodextrin-Bearing Gold Glyconanoparticles for the Development of Site Specific Drug Delivery Systems. *Langmuir* **2014**, *30*, 234−242.
(60) Chen, X.; Zhang, Z.; Liu, J.; Wang, L. A polymer Electron Donor based on Isoindigo units Bearing Branched Oligo(ethylene Glycol) Side Chains for Polymer Solar Cells. *Polym. Chem.* **2017**, *8*, 5496−5503.
(61) May, F.; Marcon, V.; Hansen, M. R.; Grozemac, F.; Andrienko, D. Relationship between Supramolecular Assembly and Charge-Carrier Mobility in Perylenediimide Derivatives: TheIimpact of Side Chains. *J. Mater. Chem.* **2011**, *21*, 9538−9545.
(62) Ochi, R.; Perur, N.; Yoshida, K.; Tamaoki, N. Fast Thermal *cis*−*trans* Isomerization Depending on pH and Metal Ions of Water-Soluble Azobenzene Derivatives Containing a Phosphate Group. *Tetrahedron* **2015**, *71*, 3500−3506.
(63) Goulet-Hanssens, A.; Utecht, M.; Mutruc, D.; Titov, E.; Schwarz, J.; Grubert, L.; Bléger, D.; Saalfrank, P.; Hecht, S. Electrocatalytic $Z \rightarrow E$ Isomerization of Azobenzenes. *J. Am. Chem. Soc.* **2017**, *139*, 335−341.
(64) Goulet-Hanssens, A.; Rietze, C.; Titov, E.; Abdullahu, L.; Grubert, L.; Saalfrank, P.; Hecht, S. Hole Catalysis as a General Mechanism for Efficient and Wavelength-Independent $Z \rightarrow E$ Azobenzene Isomerization. *Chem.* **2018**, *4*, 1740−1755.
(65) Hallett-Tapley, G. L.; D'Alfonso, C.; Pacioni, N. L.; McTiernan, C. D.; González-Béjar, M.; Lanzalunga, O.; I, A. E.; Scaiano, J. C. Gold Nanoparticle Catalysis of the *cis*−*trans* Isomerization of Azobenzene. *Chem. Commun.* **2013**, *49*, 10073−10075.

DOI: 10.1021/jacs.8b09638
J. Am. Chem. Soc. XXXX, XXX, XXX−XXX

(66) Titov, E.; Lysyakova, L.; Lomadze, N.; Kabashin, A. V.; Saalfrank, P.; Santer, S. Thermal Cis-to-Trans Isomerization of Azobenzene-Containing Molecules Enhanced by Gold Nanoparticles: An Experimental and Theoretical Study. *J. Phys. Chem. C* **2015**, *119*, 17369−17377.
(67) Simoncelli, S.; Aramendía, P. F. Mechanistic Insight into the *Z*−*E* Isomerization Catalysis of Azobenzenes Mediated by Bare and Core−Shell Gold Nanoparticles. *Catal. Sci. Technol.* **2015**, *5*, 2110−2116.
(68) Dennington, R.; Keith, T. A.; Millam, J. M. *GaussView 5*, version 5.0.8; Semichem Inc.: Shawnee Mission, 2009.
(69) Döbbelin, M.; Ciesielski, A.; Haar, S.; Osella, S.; Bruna, M.; Minoia, A.; Grisanti, L.; Mosciatti, T.; Richard, F.; Prasetyanto, E. A.; De Cola, L.; Palermo, V.; Mazzaro, R.; Morandi, V.; Lazzaroni, R.; Ferrari, A. C.; Beljonne, D.; Samorì, P. Light-Enhanced Liquid-Phase Exfoliation and Current Photoswitching in Graphene-Azobenzene Composites. *Nat. Commun.* **2016**, *7*, 11090.
(70) Klajn, R.; Wesson, P. J.; Bishop, K. J. M.; Grzybowski, B. A. Writing Self-Erasing Images using Metastable Nanoparticle "Inks". *Angew. Chem., Int. Ed.* **2009**, *48*, 7035−7039.
(71) Sharma, S.; Kim, B.; Lee, D. Water-Soluble Pd Nanoparticles Capped with Glutathione: Synthesis, Characterization, and Magnetic Properties. *Langmuir* **2012**, *28*, 15958−15965.
(72) Amstad, E.; Gillich, T.; Bilecka, I.; Textor, M.; Reimhult, E. Ultrastable Iron Oxide Nanoparticle Colloidal Suspensions Using Dispersants with Catechol-Derived Anchor Groups. *Nano Lett.* **2009**, *9*, 4042−4048.
(73) Garcia-Amorós, J.; Sánchez-Ferrer, A.; Massad, W. A.; Nonell, S.; Velasco, D. Kinetic Study of the Fast Thermal *cis*-to-*trans* Isomerisation of *para*-, *ortho*- and Polyhydroxyazobenzenes. *Phys. Chem. Chem. Phys.* **2010**, *12*, 13238−13242.
(74) Garcia-Amorós, J.; Velasco, D. Understanding the Fast Thermal Isomerisation of Azophenols in Glassy and Liquid-Crystalline Polymers. *Phys. Chem. Chem. Phys.* **2014**, *16*, 3108−3114.
(75) Poutanen, M.; Ahmed, Z.; Rautkari, L.; Ikkala, O.; Priimagi, A. Thermal Isomerization of Hydroxyazobenzenes as a Platform for Vapor Sensing. *ACS Macro Lett.* **2018**, *7*, 381−386.
(76) Dunn, N. J.; Humphries, W. H.; Offenbacher, A. R.; King, T. L.; Gray, J. A. pH-Dependent *Cis* → *Trans* Isomerization Rates for Azobenzene Dyes in Aqueous Solution. *J. Phys. Chem. A* **2009**, *113*, 13144−13151.
(77) Bléger, D.; Hecht, S. Visible-Light-Activated Molecular Switches. *Angew. Chem., Int. Ed.* **2915**, *54*, 11338−11349.
(78) Klajn, R. Spiropyran-based dynamic materials. *Chem. Soc. Rev.* **2014**, *43*, 148−184.
(79) Qian, H.; Pramanik, S.; Aprahamian, I. Photochromic Hydrazone Switches with Extremely Long Thermal Half-Lives. *J. Am. Chem. Soc.* **2017**, *139*, 9140−9143.
(80) Haase, M.; Schaefer, H. Upconverting Nanoparticles. *Angew. Chem., Int. Ed.* **2011**, *50*, 5808−5829.

DOI: 10.1021/jacs.8b09638
J. Am. Chem. Soc. XXXX, XXX, XXX−XXX